The Role of Structural Carbon in Transition Metal Sulfides Hydrotreating Catalysts

Gilles Berhault, Apurva Mehta, Alexadru C. Pavel, Jianzhong Yang, Luis Rendon, Miguel José Yácam, Leonel Cota Araiza, Alberto Duarte Moller, Russell R. Chianelli

The necessity of improving the hydrotreating sulfide catalysts' efficiency in deep hydrodesulfurization (HDS) is urgent due to new environmental regulations regarding sulfur content in fuels. Progress has been made in understanding the basis for cobaltpromoted molybdenum sulfide activity. However, recent results [R. R. Chianelli and G. Berhault, Catal. Today 53, 357 (1999)] have evidenced that carbon plays an important role in the stabilized structure of active catalysts. Indeed, the active surface in the stabilized, catalytically active transition metal sulfide (TMS) phase is carbided. Moreover, it is well-known that organosulfide treatment of oxide catalysts to produce the active catalytic form results in a better HDS activity, suggesting an initial modification of the sulfide structure in the presence of a carbon source. This study reports the structural and textural modifications of unsupported MoS_2 catalyst via Ch_3-S-CH_3 or dibenzothiophene treatment in order to better characterize the formation of structural carbon on MoS_2 layered particles. Both bulk characterization techniques (Synchrotron X-ray diffraction, far-IR) and surface-sensitive methods (electron energy loss spectroscopy (EELS), near-edge X-ray absorption fine structure (NEXAFS)) were performed in order to carefully study the final state of carburized unsupported molybdenum sulfide. Complementary electronic microscopy studies were carried out to clarify textural modifications occurring consecutively with this treatment. Evidence is

shown that structural carbon processes through a replacement of sulfur atoms at the reactive edges of MoS_2 platelets resulting in a stabilized $MoS_{2-x}C_x$ phase. This carburization surface process does not affect the MoS_2 bulk structure. Results also demonstrate that carbon stabilizes texturally sulfide particles, keeping crystallites smaller and less stacked. Thus, the active TMS should be viewed as sulfide-supported transition metal carbides. This work is a preliminary study about the neglected role of carbon on TMS-based catalysts operating in hydrotreating conditions. Further studies will point out the catalytic consequences due to the formation of this stabilized phase.

Introduction

Since Weisser and Landa wrote their classic book “Sulfide Catalysts: Their Properties and Applications” (1) more than 20 years ago, considerable progress has been made in understanding the basis for the activity and selectivity of Mo- and W-based hydrotreating catalysts. Since the 1970s, different models were proposed to explain the promoter effect of Co or Ni on alumina-supported MoS_2 or WS_2 (2–5). But, the first physical proof of a specific cobalt environment was presented by Topsøe and his group (6): Co atoms are located on the edges of MoS_2 platelets giving rise to a specific mössbauer signal, the “CoMoS” phase, different from the usual signal for Co_9S_8.

This description of the active phase was based on several characterization measurements (EXAFS, Mössbauer, XPS,…) made on fresh catalysts or on catalysts contacted with model compounds in a gas phase reactor. However, catalysts stabilized in the hydrotreating process environment contain structurally important carbon that has been ignored in describing sulfide catalysts (7). An industrial catalytic unit is a triphasic

reactor with a solid catalyst, hydrogen gas, and a liquid phase composed of a complex mixture of hydrocarbons. Before being dissociatively chemisorbed on the catalyst surface, hydrogen must diffuse from the gas phase to the liquid one, solubilize, and then diffuse from the liquid phase to the catalyst surface. In such an environment, the surface of this sulfide catalyst is exposed to a lower hydrogen concentration than expected and to a very high partial pressure of “carbon” compounds. In this case, the sulfide form must be considered a precursor state that leads to an active phase structurally containing carbon. Early evidence for the importance of structural carbon was found in the studies made by Chianelli and Pecoraro (7–9). A RuS_2 catalyst stabilized 1000 h in a catalytic environment exhibited a $RuS_{2-x}C_x$ from with carbon replacing sulfur atoms on the surface. Seiver and Chianelli (10) showed that the layered transition metal sulfides (TMS) presented the same behavior. By using $(NR_4)_2MoS_4$ (*R*=alkyl group) as a precursor for catalyst preparation, the activity was found to b higher that with catalysts prepared conventionally with ammonium heptamolybdate, $(NH_4)_6Mo_7O_{24}$. This increase of activity was related to the presence of alkyl groups in the precursor, wich increased the inclusion of structural carbon in the operating catalyst (7). Ramachandran and Massoth(11) have also suggested that the hydrodesulfurization mechanism can present sulfur-containing carbonaceous intermediates. Using ^{14}C Ragiotracer elements, Busell and Somorjai (12) showerd that the clean Mo (100) surface of a single crystal can change in a carbided surface with carbon atoms in a fourfold hollow site.

Furthermore, the role of carbon on these sulfide solids can be assessed at different steps of the hydrotreating process. Commercial catalysts are sold in an inactive oxide form and the sulfide active phase is obtained by a pretreatment using different

sulfiding agents, i.e.,H_2S,RSH,$CH_3–S–CH_3$, $CH_3–S–S–CH_3$ (DMDS), or other alkylpolysulfides, or directly in situ by the feed to treat. Hallie (13) has shown a strong dependency of the hydrodesulfurization (HDS) activity on the nature of the sulfiding agent. Consequently, the objective of this work is to better understand the interaction chemistry between transition metal sulfide catalysts and sulfur-containing organic molecules. Indeed, even if the role of carbon in operating Mo-based TMS has been largely ignored due to the analytical difficulties involved, understanding the basic properties of TMS catalysts cannot progress further without developing this knowledge. For this purpose, unsupported molybdenum sulfide solids were treated in the presence of $CH_3–S–CH_3$ and characterized by using both bulk and surface physicochemical techniques. This will lead us to present evidence that the structural carbon which forms is an essential part of the stabilized active catalyst with a carbidic nature. Subsequently, active catalysts should be viewed as sulfide-supported transition metal carbides (14).

Experimental

Catalyst Preparation

Synthesis of the $(NH_4)_2MoS_4$ precursor. A 4.0-g quantity of $(NH_4)_6[Mo_7O_{24}]. 4H_2$ (Mallinckrodt) was dissolve in 20 mL of water. An excess of high concentrated ammoniu sulfide aqueous solution (32.0 g) was then added a room temperature (RT) to the ammonium molybdate solution [(NH4)2S, 42.5% in aqueous solution (Strem Chemicals)]. The solution became immediately red–orange and was heated moderately at 333 K. After 1 h, the solution was cooled down in an ice bath without stirring and kept at this temperature for 3 h. Precipitated red crystals of $(NH_4)_2MoS_4$ appeared. Crystals were then filtered and washed several times with isopropanol, followed by drying in air.

The conversion was80%inMocontent and the purity of the product was checked by IR spectroscopy and X-ray diffraction.

Thermal decomposition of $(NH_4)_2MoS_4$ into MoS_{2+X}. The precursor was thermally decomposed under N_2 at a given temperature for 2 h (heating rate 2.5 K . min^{-1}, N_2 flow: 60 cm^3 . min^{-1}). The temperature of the thermal treatment was modified in order to vary the crystallinity of the MoS_{2+x} samples as well as the S/Mo ratio. The thermal decomposition of the ammonium tetrathiomolybdate (ATTM) precursor was carried out in different steps between 393 and 533 K under an inert atmosphere. First, the thiosalt precursor was decomposed into the amorphous molybdenum trisulfide phase (15) according to the following process:

$(NH_4)_2MoS_4 \rightarrow MoS_3+2NH_3+H_2S$.

At temperatures higher than 573 K, MoS_{2+X} were obtained by autoreduction from MoS_3 (the value of *X* decreases with increasing temperature until pure MoS_2 is obtained). After this treatment, the solids were cooled down to RT under N_2 and stored in sealed bottles. Samples were labeled MST with *T* (in *K*) temperature of treatment under N_2.

Dimethylsulfide thermal treatment. MoS_{2+x} samples (100 mg) were flushed under N_2 at RT for 15 min before being contacted with a mixture of $CH_3–S–CH_3$ (DMS) diluted in N2 or H2. Two different partial pressures were chosen: 180 and 470 Torr (24.0 and 62.7 kPa). The solids were then heated under this flowing reactant mixture up to a given temperature (573 K<*T*<833 K) at a heating rate of 2.5 K . Min^{-1} and maintained at this temperature for 1 h. The samples were cooled down to RT in the presence of the $N_2(H_2)/CH_3–S–CH_3$ mixture, flushed 2 h with N_2, and stored in sealed bottles under Ar.

Elemental analysis (Mo, S, and C contents) was performed by Galbraith Laboratories, Inc. Sulfur content overestimation was corrected using a very highly crystallized MoS_2 sample as reference.

Synthesis of dibenzothiophene (DBT)-treated unsupported MoS_2. The carburization process can be further increased by directly preparing a MoSXCy sample in a bomb in the presence of a dibenzothiophene/decalin mixture. Therefore, 1 g of ATTM was charged in the bomb and was mixed with the DBT solution, prepared by dissolving 4.4 g of dibenzothiophene in 100 cm^3 of hot decalin. The temperature was then increased up to 623 K and maintained for 3 days. The bomb was then progressively cooled down to RT in 1 day. The sample was then carefully washed with toluene before being dried overnight at 323 K. This sample reflected the effect of carburization under catalytic conditions.

FTIR Spectroscopy

The samples were characterized by infrared spectroscopy in the 4000- to 200-cm^{-1} range. Pellets were prepared by diluting the sample in CsI powder (Wilmad, Infrared Grade) in a1%mass ratio. CsI powder was preferred due to its high transparency in the far-infrared region (until 180cm^{-1}).The IR spectra were recorded using an ATI Mattson Infinity 60 AR spectrometer. Far-infrared domain (<500 cm^{-1}) as well as mid-IR regions were inspected with a DTGS detector equipped with a PE window and a CsI beamsplitter. Spectra were recorded in the 2000- to 180-cm^{-1} region. For higher wavenumbers domains, acquisitions were carried out by switching to a KBr beamsplitter. Band intensities were corrected for slight differences in weight. Spectrum treatment was carried out using the IR Winfirst software.

Synchrotron X-Ray Diffraction

Experiments were performed at the Stanford Synchrotron Radiation Laboratory on beamline 2-1. The high brightness and vertical collimation of the synchrotron beam allow the use of a Si(111)-based detector able to resolve lattice changes of the order of 0.1%. The size of the focused beam is 2x1 mm and approximately 10^{11} photons/s are incident on the sample at an energy of $1.0x10^4$ eV. The XRD patterns were collected in the 4–104° 2Θ range with an increment of 0.1°. The synchrotron source was used to determine structural differences before and after the carbiding process.

Transmission Electron Microscopy

The MoS2 samples were suspended in isopropanol using an ultrasonic bath. A drop of solution was placed on a 200-mesh copper grid and air-dried. Samples were examined using a JEOL 4000-EX high-resolution microscope. Some of the images were computer processed to increase the signal-to-noise ratio. Particle size distribution was determined by counting 600–700 particles. The average particle size was calculated according to the first moment of the distribution:

$$\frac{\sum_{i=1}^{n} n_i L_i}{\sum_{i=1}^{n} n_i},$$

With *L* representing the length of aMoS_2 slab as determined directly on pictures, corresponding to the diagonal of a slab; *n* is the number of particles measured in a size range or stacking number of index *i*.

Electron Energy Loss Spectroscopy

The samples were ultrasonically dispersed in ethanol. A drop of the suspension was then placed in a holey carbon Cu grid. The observations were performed with a

JEOL 2010 transmission electron microscope equipped with a Gatan 666 parallel spectrometer. Special care was taken to observe the areas of interest through the holes in the carbon film. Attention was particularly devoted to the C K-edge transition region around 300 eV.

Near-Edge X-Ray Absorption Fine Structure (NEXAFS)

The NEXAFS experiments were carried out at the Stanford Synchrotron Radiation Laboratory by Dr. Joachim Stöhr and will be the subject of a future report. The NEXAFS spectra were recorded as a function of the incident X-ray photon energy in the vicinity of theCK-edge (275–325 eV). The electron-yield intensity was measured. This method is sensitive only to the surface layers with a mean free path of about 10 Å, yielding information very similar to Auger Electron and X-ray Photoelectron techniques.

Molecular Simulation

The Crystal Builder, Surface Builder, Interface Builder, Force-Field, IR/Raman, and Diffraction Crystal an Rietveld (DBWS) modules of the Cerius^2 4.0 simulation package of Molecular Simulation, Inc. (MSI), were used to compare experimental XRD and IR results with a theoretical model of the structure and stability of bulk MoS_2. The crystalline models were generated using the Crystal Builder module (MoS_2 atomic positions, symmetry conditions, and lattice parameters). The minimum energy configuration was calculated using a Force-Field Westheimer method based on the Born–Openheimer approximation. The particle size determined by HREM was used in order to build hexagonal MoS2 particles and lattice parameters were optimized in order to fit with XRD and IR results.

Results

Infrared Characterization

Figure 1 reports the evolution of IR spectra recorded at different temperatures of DMS treatment under N_2 or H_2 atmospheres. The MoS_2 sample obtained by ATTM thermal decomposition at 833 K (MS833) presents two main bands at 385 and 467 $cm^{-1.}$ According to Chang and Chan (16) and Wieting and Verble (17), the 385- and 467-cm^{-1} bands are assigned to the Mo–S stretching modes of vibration. The presence of two *v*(Mo-S) signals is related to the layered nature of the MoS_2 crystallites with vibrations, respectively, along the basal plane (**E**$\perp$**c,** 385 cm^{-1}) and perpendicularly to the basal plane (**E**//**c**, 467 cm^{-1}). A decrease of the intensity of the 385-cm^{-1} signal is observed as the temperature of DMS treatment is increased. Moreover, the two Mo-S stretching bands gradually exhibit an asymmetric shape at lower wavenumbers and a slight shift to 380-381 cm^{-1}. In the mid-IR region, a broad band at 1093 cm^{-1} is observed as well as a minor signal at 830cm^{-1}, as already observed by Chang and Chan (16). These peaks are related to intermediary products of the $CH_3–S–CH_3$ decomposition as $(C_xS)_n$ polymer species (18) and they increase as the N_2 temperature increases, indicating further production of this species. A treatment of a MS833 sample at 793 K under a H_2/DMS mixture (P_{DMS}=180 Torr (24.0 kPa)) involves the disappearance of any signal in the mid-IR region, indicating a removal of the polymeric species. However, the asymmetric tail remains with some new features that require further study. These results show that a DMS treatment is followed by the appearance of an asymmetric tail at lower energy in both the parallel and the perpendicular Mo–S stretch. We believe that this asymmetric tail is due to both carbon incorporated into the MoS_2 structure and increased bending and folding of the MoS2 layers (14, 19).

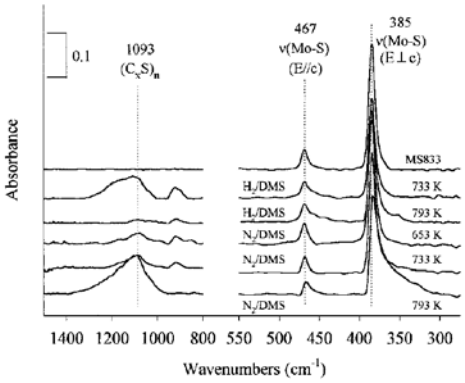

FIG. 1. Evolution of the IR spectra of unsupported MoS_2 samples recorded at different temperatures of DMS treatment under a N_2 (or H_2) atmosphere in the mid-IR wavenumbers region (1400–800 cm^{-1}) and in the far-IR region (550–300 cm^{-1}).

Elemental Analysis

Table 1 reports the Mo, S, and C content of different MS833 (the standard preparation described above) samples treated with DMS in the presence of a N_2 or H_2 atmosphere at 793 K for two different DMS partial pressures. Increasing the DMS partial pressure results in a slight decrease in S content. Meanwhile, the C content strongly increases and a very large excess is observed with a stoichiometry of $MoS_{1.96}C_{1.71}$ after treatment at 793 K and 470 Torr (62.7 kPa) ofDMS. Using hydrogen reduces both sulfur and carbon content. The final overall (SCC)/Mo ratio is equal to the initial S/Mo ratio before treatment in this sample. Taking into account that no signal is detected at 1093cm^{-1} ((formation of carbosulfide polymer species), this result suggests the replacement of some S atoms by C inside theMoS_2 structure whenH_2/DMS is used as a treatment. The sample produced in hydrogen is most representative of a catalyst treated under catalytic conditions.

Synchrotron X-Ray Diffraction

A monochromatic beam (λ=1.2389 Å) was used to record a XRD pattern of a MS833 sample (MoS_2–833 K–ATTM decomposition in N_2). The higher resolution and superior

signal/noise ratio of this technique were readily apparent. These experimental patterns were then fitted to a simulated pattern using the Crystal Diffraction and Crystal Builder modules from Cerius^2 4.0 (Molecular Simulations, Inc.).

Figure 2 shows XRD patterns before (upper line) and after (lower line) a DMS treatment of a MS833 sample under N_2 at 793 K (P_{DMS}=180 Torr (24.0 kPa)). No new peaks are detected; only a general twofold decrease in the absolute intensity is observed for the DMS-treated bulk MoS_2 sample with similar volumes pointing out a lower density material after DMS treatment. The background scattering at low and high angles is matched, indicating significance for the intensity differences in the remaining diffraction patterns (20). The (110) plane at 2Θ=47° presents a stronger intensity relative to the (100) plane after DMS treatment. Fitting calculations between experimental and simulated XRD patterns reveal that this relative variation of the (110) plane is related to a higher distortion (more folding) along the *c* axis after the CH_3-S-CH_3 treatment. Simulated calculations were performed by assuming that no modification of the particle size or the stacking number occurred as suggested by SRD. Synchrotron XRD measurements do not reveal the formation of a separate carbide phase but indicate clearly that a MoS_2-like bulk structure is retained after this treatment. The lower intensity shown by the DMS-treated sample and the absence of any indication of amorphous carbon scattering under the conditions of measurement indicate that some carbon has been incorporated into the structure.

TABLE 1

Mo, S, and C Contents of Different MS833 Samples Treated in the Presence of CH_3–S–CH_3 at 793 K for Two Different Partial Pressures, 180 and 470 Torr (24.0 and 62.7 kPa), with a N_2 or H_2 Atmosphere

Sample name	Treatment	Mo%	S%	C%	Stoichiometry
MS833	MoS_2–833 K	58.61	42.02	/	$MoS_{2.04}$
MS 8379 NDMS 180	MoS_2–833 K N_2/DMS 793 K 180 Torr (24.0 kPa)	53.95	39.56	7.57	$MoS_{2.05}C_{1.12}$
MS 8379 NDMS 470	MoS_2–833 K N_2/DMS 793 K 470 Torr (62.7 kPa)	53.10	37.32	11.35	$MoS_{1.96}C_{1.71}$
MS 8379 HDMS 180	MoS_2–833 K H_2/DMS 793 K 180 Torr (24.0 kPa)	60.77	39.67	1.64	$MoS_{1.82}C_{0.22}$

Note. Sulfur weight percentage was corrected to take into account overestimation of sulfur content. The correction was made by comparison to a reference: a highly crystallized MoS_2 sample with a S/Mo ratio of 2.00.

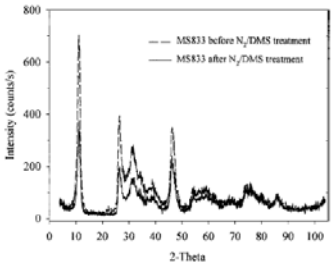

FIG. 2. Comparison of the two synchrotron XRD patterns (λ = 1.2389 Å) of a MS833 sample before (upper line) and after (lower line) a CH_3–S–CH_3 (DMS) treatment (P_{DMS} = 180 Torr (24.0 kPa), T = 793 K for 1 h, total flow = 80 cm^3/min).

Transmission Electron Microscopy

HREM studies reveal structures typical of the layered MoS_2 phase. Figure 3 presents a micrograph of a MoS_2 sample prepared by heating the $(NH_4)2MoS_4$ precursor at 833K (MS833).

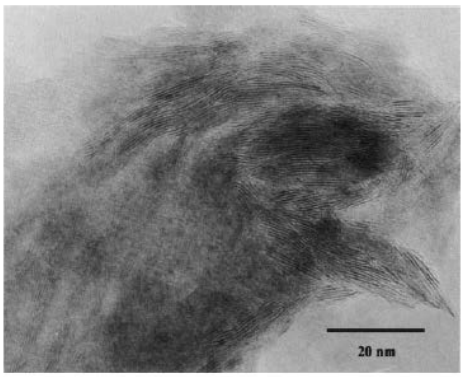

FIG. 4. HREM micrograph of a MS833 sample treated in the presence of N_2/DMS at 793 K–1 h (P_{DMS} = 180 Torr (24.0 kPa), total flow = 80 cm^3/min).

Bulk MoS2 particles appear in closely packed groups of large slabs in highly folded shapes. Statistics performed on more than 10 pictures give an average slab

length of 94 Å and a mean value for the stacking number of 9.3. These results are in a good agreement with XRD results for which an apparent stacking value of 7.8 was obtained.

Figure 4 presents a TEM micrograph of a MS833 sample treated in the presence of N_2/DMS at 793 K. HREM reveals heterogeneous regions with some highly stacked layers. Other zones present less stacked and less curved layers, which are supported on a “fluffy” carbon support. Statistics made on more than 10 different pictures and 800 particles show a very marked evolution of the particle size and the stacking number in these fluffy regions (cf. Fig. 5).

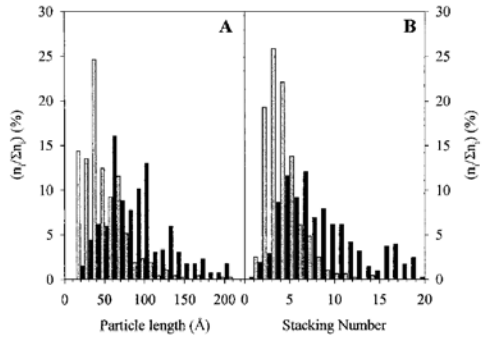

FIG. 5. Comparison between the HREM particle size and stacking number distributions of a “freshly” MS833 sample (dark histogram) and of a MS833 sample treated under N_2/DMS at 793 K–1 h (P_{DMS} = 180 Torr (24.0 kPa), total flow = 80 cm^3/min) considering “fluffy” carbon-supported MoS_2 particles.

The particle size is reduced by a factor of 2 between the freshly sulfided sample (94 Å) and the carbon-supported MoS_2 slabs (47Å). The stacking number decreases from 9.3 to 4.0. Similar results were observed after a hydrogen/DMS treatment with an average slab length of 50 Å and a stacking number of 4.2.

Electron Energy Loss Spectroscopy

Electron energy loss spectroscopy (EELS) studies are useful to distinguish between different carbon structures. EELS is directly related to the primary process of

electron excitation, in which a beam of electrons will lose a certain amount of kinetic energy by Coulomb repulsion with inner-(high loss) or outer- (low loss) shell atomic electrons of the target compound. This repulsion provokes an inelastic scattering for the transmitted electrons. EELS spectra generally record the scattered intensity as a function of the decrease in kinetic energy (21). At high-energy loss values, scattered intensity corresponds to inner-shell excitation and is characterized by edges, whose energy loss is approximately the binding energy of the corresponding atomic shell.This “ionization threshold” is directly related to a particular element. Moreover, these ionization edges possess a fine structure reflecting the energy-band structure of the studied sample. Consequently, these fine structure ionization shapes are characteristic of a given structure for a particular element. For example, Fig. 6 reports the EELS C K-edge shapes that we have recorded for different carbon structures: graphite, amorphous carbon, diamond, and β-Mo_2C (Strem Chemicals). A MS833 sample treated at 793 K with N_2/DMS (P_{DMS}=180Torr (24.0 kPa)) are reported inFig. 7. These samples show an intense carbon peak corresponding to a high carbon content in the sample. From the relative intensity of the C K-edge peak due to the π* antibonding state, the fine structure does not fit to a graphitic structure.

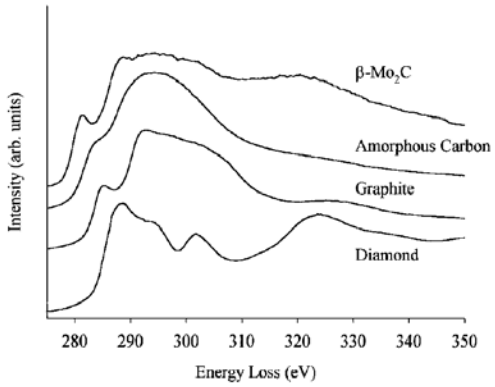

FIG. 6. EELS C K-edge (275–350 eV) shapes of different carbon structures: diamond, graphite, amorphous carbon, and β-Mo_2C.

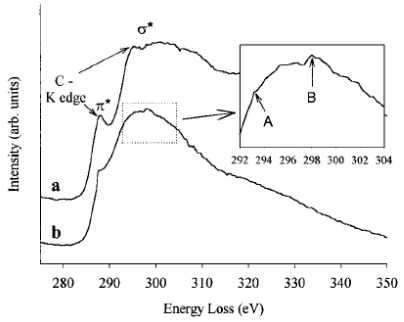

FIG. 7. EELS C K-edge shapes of (a) a β-Mo_2C reference and (b) a MS833 sample treated at 793 K with N_2/DMS at a DMS partial pressure of 180 Torr (24.0 kPa). The inset presents the fine structure shape observed at the σ^* transition.

The peak shape structure in the vicinity of the ionization edge is different than amorphous, graphite, or carbide structures. For amorphous carbon, the C K-edge peak presents a smooth shape without any detectable peak for the σ^* shape presents two features A and B. For graphite, feature A is always at higher intensity than B; for carbides and diamond, this feature is the opposite, i.e., B is at a higher intensity than A. This is due to a different density of states structure for the graphitic carbon sp^2 bonds versus tetrahedral sp^3 bonds in carbides (22). In our DMS-treated MoS_2 samples, B is higher than A. This first confirms that the structure is not graphitic and, second, that Mo–C bonds of a carbide-like structure are present. However, the π* peak appears less

sharp on our samples than on a standard molybdenum carbide sample. One may assume that a part of the carbon detected is also of an amorphous nature.

Near-Edge X-Ray Absorption Fine Structure

The DBT-treated MoS_xC_y sample was characterized by NEXAFS at the Stanford Synchrotron Radiation Laboratory and compared to a commercial β-Mo_2C Mo2Cpowder sample (Strem Chemicals). Figure 8 reports the C K-edge spectra of the molybdenum carbide reference and the MoS_xC_y sample prepared in the presence of DBT. These spectra were recorded measuring Auger electrons coming from the near surface atoms The C K-edge shapes of these two samples are almost perfectly identical with two sharp resonances at 285.0 and 288.5 eV and a broad feature at~293.0 eV. The C K-edge features are generally assigned to the excitation of the C 1s electrons to the partially filled and unfilled orbitals formed by the hybridization of C 2p orbitals with Mo 4d orbitals (23). In this respect, the two first peaks correspond to the transitions of C 1s electrons to the p-d (t_{2g}) and p-d (eg) hybridized orbitals of carbides.

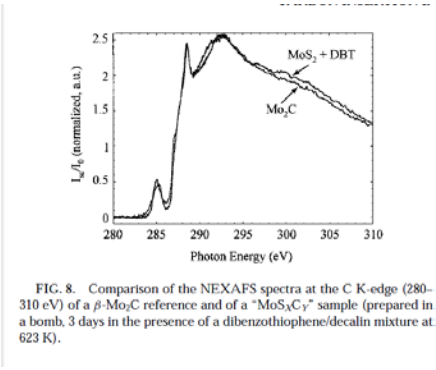

FIG. 8. Comparison of the NEXAFS spectra at the C K-edge (280–310 eV) of a β-Mo_2C reference and of a "MoS_xC_y" sample (prepared in a bomb, 3 days in the presence of a dibenzothiophene/decalin mixture at 623 K).

The broad signal at 293 eV is related to a complex electronic transition between the C 1s orbital and an unoccupied orbital involving contributions from the 2p and 3p orbitals of carbon and the d and s states of Mo (24, 25). Moreover, it should be noticed that the characteristic sharp peaks of graphite at 291.5 and 292.5 eV were not detected,

rejecting definitely the formation of an organized carbon support (26). However, further experiments using the fluorescence-yield method are still necessary to conclude definitely on the nature of the bulk phase, but the main conclusion is that the surface chemistry (the outermost layers) of a “carbided” molybdenum sulfide catalyst is equivalent to a pure Mo_2C compound.

Discussion

The carbon effect on the dispersion and the size of MoS_2 slabs has already been observed at different steps of the hydrotreating process and seems to be a general phenomenon related to the interaction of carbon-containing reactants with sulfide catalysts. For example, Labruyère et al. (27) have observed that the pretreatment of MoO_3 by alkylpolysulfides (e.g., tertiononylpentasulfide, Sulficat process, Eurecat) gives rise to smaller and less stacked crystallites. This result was also noted by Van Gestel et al. (28). Afanasiev et al. (29) have confirmed this effect by using a surfactant, cetyltrimethylammonium chloride, during the ATTM decomposition. Such a preparation involves the formation of high surface MoS2 particles constituted of only single layers. Pollack et al. (30) have observed a dramatic decrease of the stacking number between a freshly sulfide catalyst (5 to 10 layers) and the same solid after exposure to the catalytic conditions (only single layers). Finally, the use of alkylammonium tetrathiomolybdates or tetrathiotungstates (31) or naphthenate salts (32, 33) for preparing MoS_2 was found to increase the dispersion to a very large extent and help to obtain very low stacked crystallites. This formation of a carbon support could explain the higher intrinsic activity of MoS_2 particles treated in the presence of or decompose from carbon-containing compounds. Chianelli and Pecoraro (9) have observed an increase of

the HDS activity by a factor of 2.5 to 3 for carbon-containing precursors compared to a standard MoS_2 sample prepared by in *situ* decomposition of the ammonium thiomolybdate precursor. For example, the tetrabutylammonium precursor was found to be three times more active than commercial catalysts. Moreover, theseMoS2 samples formed by decomposition of alkylammonium salts generally present a high C content, as also observed in this study, suggesting that this higher activity is connected to the formation of smaller and less stacked crystallites and then to a better dispersion on a carbon support. This effect must be related to previous studies emphasizing the very good dispersion of MoS_2 particles on carbon-supported catalytic systems. Indeed, metal sulfides supported on carbon present a much higher activity than corresponding Al_2O_3-supported ones (34, 35). The DMS treatment is also accompanied by an increase of the specific surface area (48 instead of 14 m^2/g for the starting material) but also by a narrow pore volume distribution centered on a diameter value of 25 Å after a treatment with N_2/DMS and of 18 A° with a H_2/DMS mixture at 623 K. This result must be correlated to previous results obtained for DBT-treated alkylammonium precursors, for which interesting pore volume distributions were also observed (9,14). Obviously, as expected, the surface area obtained for a fresh MoS_2 catalyst presents a low value according to its high stacking number, as generally observed in gas phase preparations. However, a threefold increase of this surface area is observed after this N_2/DMS treatment. In the presence of the liquid phase, i.e., a DBT/decalin mixture, surface areas could be much higher and close to commercial catalysts' values (14). A thermal treatment in the presence of carbon then increases strongly the morphological properties of the final MoS2 particles.

Carbon also structurally modifies the sulfide catalysts.

This fact can be found in previous results of Somorjai and co-workers (12), which indicated that a Mo(100) single crystal used in the HDS of thiophene was modified into a carbided surface with carbon atoms in the same fourfold hollow sites as for sulfur atoms. Nevertheless, in contrast to sulfur, a hard base that decreases activity by blocking active sites, carbon does not hinder the interaction of thiophene with the metal active sites. The carbidic nature of the active phase is also emphasized through the different patents of Chianelli about alkylammonium tetrathiometallates (9, 36) or through the characterization of the stabilized phase of RuS_2 during a dibenzothiophene HDS test in a Carberry reactor (7). In this respect, carbide phases inherently appear highly active in hydrodesulfurization (37, 38) as well as hydrodenitrogenation (39–41).

XRDand IR experimental results do not reveal the presence of a bulk carbide phase after a treatment with DMS up to 793 K, even with high carbon partial pressures. Only a carbon support effect is detected through XRD and HREM experiments. However, due to a strong metallic character, the β-Mo_2C IR spectrum does not present any peak in the far-IR region. This “metallic character” is related to its hexagonal close-packed structure for which interstitial carbon atoms occupy only half of the octahedral holes. Therefore, metal–metal interactions occur and might explain why molybdenum carbide, and more generally many transition metal carbides, displays catalytic properties close to those found for precious metals (42–45). Moreover, the interlayer distance calculated thanks to micrographs stays unchanged after a “carbon–sulfur” treatment even in the fluffy carbon supported zones. XRD patterns do not present any

shift of the (002) peak consecutively to an intercalation of organic fragments between the layers.

On the contrary, surface-sensitive EELS techniques show the formation of Mo-C bonds at the surface of DMS-treated MoS_2 particles. Consequently, a carbiding process seems to occur by replacing some sulfur atoms by carbon without phase segregation. As the active sites are located on the edges of MoS_2 layers while the basal planes are catalytically inert (46–50), the MoS_2 active edge sites would then be first involved in this replacement.

The hypothesis of a replacement of S atoms on the edges by carbon could be ascertained through crystallographic considerations based on the model developed by Kasztelan (51). HREM studies revealed that amorphous carbon is present in a negligible amount on the MS833 sample treated with H_2/DMS at 793 K (P_{DMS}180 Torr (24.0 kPa)). Moreover, its IR spectrum (cf. Fig. 1) does not exhibit a *v* (C=S) signal. This sample is then suitable for considering a carbon replacement phenomenon. Taking into account the particle size determined by HREM for the MS833 sample, the theoretical stoichiometry calculated from the Kasztelan's model would be $MoS_{1.87}C_{0.26}$, which is very close to the $MoS1_{.82}C_{0.22}$ stoichiometry determined experimentally. However, this result assumed that the particle size is unchanged after the DMS treatment. Nevertheless, results completely sustain the hypothesis of a sulfur replacement on the edges ofMoS_2 slabs by C atoms. Based on these observations, in order to check the evidence of this carbon replacement process, experimental results were correlated to IR simulated spectra calculated using the Force-Field and IR/Raman modules of Cerius^2 4.0 (MSI, Inc.). These fitting simulations are based on direct approximate calculations

and not on density functional techniques (DFT). However, the layered MoS_2 particles were built taking into account former DFT studies on this subject, mainly by Faye et al. (52) and Raybaud et al. (53), on $Mo_{12}S_{24}$ clusters and relaxation effects along the (10 $\bar{1}$0) plane, respectively. Our objective is to build MoS2 layers with particles sizes as close as possible to the real particle size generally determined for these solids by HREM techniques (25–100 Å or more). Consequently, the number of atoms involved in these calculations could be very important and requires a large amount of computational time by DFT techniques.

In a first step, the crystallographic structure of our samples was refined by comparing both experimental and simulated spectra. 2-H and 3-R stacking sequences data corresponding to hexagonal or rhombohedral structures were compared. No differences were detectable and 2-H crystallographic data were chosen for further calculations (54). Two parameters appear to be critical in the evolution of the vibrational frequencies of the *v* (Mo–S) bonds, i.e., the c/a axial ratio and the internal parameter *z*.

TABLE 2

Comparison of the *c*/*a* Axial Ratio, the Internal Parameter *z*, the Atomic Volume *A*, and the Different Mo–S and S–S Bond Distances of a 2H-MoS_2 for IR Fitted, Experimental, and Density Functional (DFT) Results (Based on Ref. 55)

								Atomic coordinates				
2H-MoS_2		Bravais class (Hexagonal)		Space group ($P6_3/mmc$ (194))				Mo (2*c*) (1/3, 2/3, 1/4)		S (4*f*) (1/3, 2/3, $z+1/2$)		
Volume (Å^3/atom)				Axial ratio c/a				Atomic parameter z				
Sim	Exp	GGA	LDA	Sim	Exp	GGA	LDA	Sim	Exp	GGA	LDA	
17.72	17.72	18.25	16.66	3.89	3.89	3.97	3.83	0.124	0.121	0.126	0.119	
d(Mo–S) (Å)		d(S–S) (Å) (within a layer)				d(S–S) (Å) (intralayer)				d(S–S) (Å) (interlayer)		
Sim	Exp	Sim	Exp	GGA	LDA	Sim	Exp	GGA	LDA	Sim	Exp	GGA	LDA
2.39		3.16	3.16	3.17	3.11	3.08	2.98	3.17	2.83	3.56	3.66	3.62	3.60

Note. Simulated unit cell dimensions: $a = 3.16$ Å, $c = 12.294$ Å.

Table 2 summarizes the crystallographic data for the molybdenite structure and compares fitting results with experimental and calculated parameters based on local

density approximation to density functional theory with or without nonlocal corrections in the form of generalized-gradient approximation (55). Hence, calculations based on the crystal unit cell show a very good fitting between experimental and simulated results with the two expected peaks due to the *v* (Mo-S) stretching modes at 385 and 467 cm^{-1}. Consequently, in a first approximation, these simple calculations are sufficient to fit correctly with experimental infrared Mo–S stretching frequencies. Hexagonal layers are then built starting from this reference file considering 2*n* units cells along the (*x, y*) plane. Layers being definite structures, hexagonal stacked MoS_2 particles are then obtained by generating a nonperiodical superstructure and by cutting the layers along the (110) plane. The as-built layers present alternating edge planes of unsaturated Mo or S atoms with *n* hexagonal cells on each side. An example of a 60-Å hexagonal layer is shown Fig. 9. Based on the previous results by Raybaud et al. (53), only slight relaxation processes are observed in vacuum on these bulk-terminated edges. The average bond length at the surface of the MoS_2 catalyst is then hardly changed, as already observed by EXAFS techniques (56). Consequently, rough calculations are then applied without considering these slight modifications. However, it is important to note that these S edges atoms are generally very reactive toward their surrounding atmosphere and could form some oxidized moieties, as already demonstrated for RuS_2 (57) on which S–S–O terminations were detected.

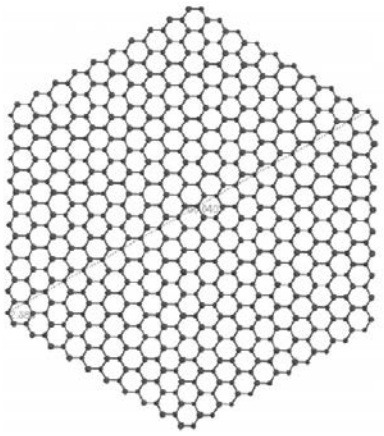

FIG. 9. Example of a 60-Å MoS_2 hexagonal layer with 10 hexagonal units on each side of the hexagonal structure (number of atoms: 900). The MoS_2 diameter is defined as the diagonal of the hexagon ($L = 2a$ with a length of a hexagonal edge).

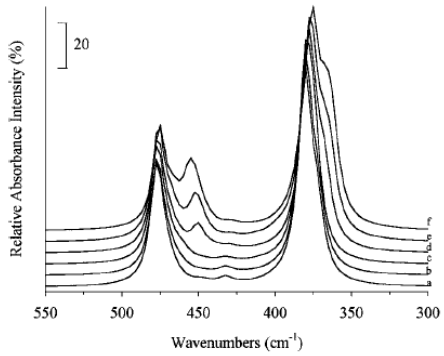

FIG. 10. Evolution of the far-IR simulated spectra (300–550 cm^{-1}) of a progressively carbided 60-Å hexagonal single layer. A "cherry model" and topotactic growth is considered for the carburization process. Spectrum (a), pure sulfidic MoS_2 sample; (b), only unsaturated S edges atoms are replaced by carbon; (c), complete carburization of the first outermost row; (d) to (f), one additional inner sulfur row is successively replaced by carbon.

The evolution of the IR simulated spectra for a progressive replacement of S atoms by C on a MoS_2 single particle is reported Fig. 10. According to their lower coordination number, edges presenting unsaturated S atoms (the $(10\bar{1}0)$ plane) are first considered the most likely reactive, as already reported by Somorjai and his group using Auger spectroscopy (49, 50). If a "cherry model" is assumed as for oxidation reactions (50), a progressive C replacement starting from the edges and slowly progressing inside the bulk structure could be envisaged. Moreover, since XRD does

not detect any structural modification after carburization, one would conclude that if the bulk structure should be carbided under these experimental conditions, this would occur through a topotactic way as observed by Lee *et al*. for MoO_3 converted into α-MoC_{1-x} (58). A progressive carburization is then envisaged starting from these unsaturated S edges, second with the Mo unsaturated edges, and, afterward, by a progressive replacement of the inner neighbors row after row. On the pure sulfide phase, two main peaks are present at around 380 and 474 cm^{-1} for the first model corresponding to a particle size of 28Å. However, the frequency of the *v* (Mo-S) (**E**//**c**), originally detected on an infinite MoS_2 unit cell at 468 cm^{-1} is shifted upward to 474 cm^{-1}. This is due to the absence of the stabilizing Van der Waals forces when considering a single layer. In fact, complementary calculations starting from a constant particle size with increasing stacking numbers confirm this fact since the *v* (Mo–S) (**E**//c) shifts to a value of 468 cm^{-1} for stacking number higher than 4.

As soon as the outermost rows are replaced by carbon, an asymmetric shape appears for the two *v* (Mo–S) stretching modes at lower wavenumbers. But, no new IR peaks are detected as long as only the first outermost row is concerned by the C replacement. To replace S by C in the second outermost row involves the appearance of a peak at 451 cm^{-1}, wich shifts up to 459 cm^{-1} as far as the C replacement is increased row after row. The asymmetric shape of the 380-cm^{-1} peak becomes progressively more marked and is characterized by a shoulder at 366 cm^{-1} while the *v* (Mo-S) vibration frequency shifts progressively from 380 to 372 cm^{-1}. After the replacement of more than five rows, the Mo–S stretching signals vanish and only the new peaks at 366 and 459 cm^{-1} are detected. However, experimentally, the absence of

any signal at 451 cm^{-1} on the DMS-treated samples suggests that only surface S atoms on the edges are replaced by C, as already proposed through elemental analysis coupled with crystallographic modelization. The asymmetric shape observed is then probably due to the formation of Mo–C bonds at the surface. Nevertheless, since no IR band was detected on β-Mo_2C due to the metallic character of this compound, the detection of a *v* (Mo–C) signal would be due to the fact that the carbide phase is supported on a MoS_2 bulk structure, well-known to possess semi-conducting properties (59). This could be predicted taking into account previous results about the reducibility of MoS_2 bulk catalysts. Unsupported MoS_2 catalytic systems are very stable and lose only a few percent of their sulfur content upon reduction at temperatures as high as 1000 K. This corresponds to the elimination of some sulfur species located at the edges of this lamellar structure (60). Then, the low reactivity of the bulk S atoms would explain why only edge sulfur species are concerned by this carbon replacement. These results suggest a progressive modification of the nature of a molybdenum sulfide particle when used in a hydrotreating reactor with a carburization process starting from the surface and progressively modifying the bulk structure. This observation is similar to the cherry model generally invoked in the case of the interaction of hydrogen with sulfide catalytic systems (61). Indeed, bulk sensitive techniques used in this study do not detect any significant modification of the MoS_2 structure while surface sensitive techniques (EELS, NEXAFS, and to a certain extent far-IR) clearly underline the formation of a carbide phase. Therefore, this study emphasizes the distinction between bulk compounds and active surface structure. It shows that the “stabilized” active phase in a hydrotreating reaction is in fact a sulfide-supported transition metal carbide (14). The absence of any

real difference between XRD patterns of a freshly “sulfided” MoS2 sample and a “sulfocarbide” one, even prepared in the presence of a high pressure in hydrocarbons, could be related to an epitaxial modification during the carbon replacement. Previous results obtained by Lee *et al.* (58) showed that molybdenum carbide synthesis from MoO_3 occurs through a topotactic process in which the synthesized metastable α-MoC_{1-x} phase exhibits pseudomorphism with the original platelets of MoO_3.

Conclusion

This study shows that sulfur terminated edges of unsupported MoS_2 catalyst are very reactive toward hydrocarbon. Indeed, a sulfur replacement by carbon can occur even using an organosulfur compound like $CH_3–S–CH_3$. It is noteworthy in this respect that sulfur species coexisting in a MoS_2 compound present very different reactivities. Completely coordinated bulk sulfur atoms are largely less reactive and are not replaced easily by carbon except in the presence of severe experimental conditions (high H_2 and HC pressures, high temperatures). Moreover, a pronounced carburization of the bulk structure would induce phase segregation with formation of a separated carbide phase, which is not observed when only the surface sulfur atoms are replaced. In fact, unsupported MoS_2 catalyst treated under the experimental conditions used in this study is rather a sulfocarbide entity with the carbide modification located mainly at the edges whereas a sulfidic bulk structure is preserved. This could constitute the first part of an explanation about the nature of the stabilized phase encountered under the hydrotreatment conditions. Indeed, a direct proportionality was observed between the initial amount of overstoichiometric sulfur and the final amount of carbon present on the

stabilized active phase. Consequently, running hydrotreating Mo-based catalysts can be seen as sulfide-supported transition metal carbides.

Moreover, treating unsupported molybdenum sulfide in the presence of CH3–S–CH_3 involves not only structural modifications but also morphological consequences. As also generally observed with any “carbon” reactant, a CH_3–S–CH_3 treatment reduces both particle size and stacking number of the final Mo catalyst, increasing the dispersion of the active phase. The as-carbided solid presents a better textural stability. This would explain the higher HDS activity measured on Mo-based catalysts pretreated in the presence of organosulfur compounds, i.e., CH_3–S–CH_3, CH_3–S–S–CH_3, or other alkylpolysulfides.

These results emphasize the high MoS_2 affinity for carbon, as already noticed in high vacuum experiments for which it is virtually impossible to avoid reaction between freshly sulfided MoS_2 and carbon residues. A sulfide catalyst exposed to a high pressure of hydrocarbons is not unchanged but reacts with surrounding carbon compounds to form a stabilized phase with a carbide-like surface chemistry.

These observations are a preliminary study about the interaction between carbon and transition metal sulfides. Further complementary studies are necessary in order to know causes and consequences of the formation of this stabilized phase, mainly from a catalytic point of view.

Acknowledgments

This work was supported by a grant from the Robert A. Welch Foundation, by the National Science Foundation, and by the General Electric Faculty for the Future.G. Berhault and R. R. Chianelli would like to thank Dr. G. Alonso Nuñez from CIMAV

(Centro de Investigaciones en Materiales Avanzados), Departamento de Catálisis, Chihuahua, Chih., Mexico, for his help. We also thank Dr. Joachim Stöhr of the Stanford Synchrotron Radiation Laboratory for providing the NEXAFS data.

References

1. Weisser, O., and Landa, S., in “Sulphide Catalysts: Their Properties and Applications, Pergamon, New York, 1973.

2. Voorhoeve, R. J. H., J. Catal. 23, 236 (1971).

3. Voorhoeve, R. J. H., and Stuiver, J. C. M., J. Catal. 23, 228 (1971).

4. Farragher, A. L., “Symposium on the Role of Solid State Chemistry in Catalysis,” ACS Meeting, New Orleans, LA (1977).

5. Hagenbach, G., Courty, Ph., and Delmon, B., J. Catal. 31, 264 (1973).

6. Topsøe, H., Clausen, B. S., Candia, R., Wivel, C., and Morup, S., J. Catal. 68, 433 (1981).

7. Chianelli, R. R., and Pecoraro, T. A., U.S. Patent 4288422 (1981).

8. Pecoraro, T., and Chianelli, R. R., J. Catal. 67, 430 (1981).

9. Chianelli, R. R., and Pecoraro, T. A., U.S. Patent 4,528,089 (1985).

10. Seiver, R. L., and Chianelli, R. R., U.S. Patent 4,430,443 (1984).

11. Ramachandran, R., and Massoth, F. E., Can. J. Chem. Eng. 60, 17 (1982).

12. Bussell, M. E., and Somorjai, G. A., J. Catal. 106, 93 (1987).

13. Hallie, H., “Ketjen Catalysts Symposium,” p. 58, Amsterdam, 1982.

14. Chianelli, R. R., and Berhault, G., Catal. Today 53, 357 (1999).

15. Walton, R. I., Dent, A. J., and Hibble, S. J., Chem. Mater. 10, 3737 (1998).

16. Chang, C. H., and Chan, S. S., J. Catal. 72, 139 (1981).

17. Wieting, T. J., and Verble, J. L., Phys. Rev. B 3, 4286 (1971).

18. Krebs, V. B., and Gattow, G., Z. Anorg. Allg. Chem. 338, 225 (1963).

19. Santiago, P., Mendoza, D., Espinosa, A., Ascencio, J. A., Yacamán, M. J., Chianelli, R. R., and Berhault, G., J. Mater. Res., in press (2001).

20. Chianelli, R. R., Int. Rev. Phys. Chem. 2, 127 (1982).

21. Egerton, R. F., "Electron Energy Loss Spectroscopy in the Electron Microscope," Plenum Press, New York, 1986.

22. Disko,M.M., Ahn,C.C., and Fultz,B.,"Transmission Electron Energy Loss Spectrometry in Materials Science," Booknews Inc., Portland,

OR, 1992.

23. Kapoor, R., Oyama, S. T., Fru¨hberger, B., De Vries, B. D., and Chen, J. G., Catal. Lett. 34, 179 (1994).

24. Pflüger, J., Fink, J., and Schwarz, K., Solid State Commun. 55, 675

(1985).

25. Chen, J. G., Frühberger, B., Eng, J., Jr., and Bent, B. E., J. Mol. Catal. A Chem. 131, 285 (1998).

26. Stöhr, J., "NEXAFS Spectroscopy," Springer-Verlag, New York, 1991.

27. Labruére, F., Dufresne, P., Lacroix, M., and Breysse, M., Catal. Today

43, 111 (1998).

28. Van Gestel, J., Leglise, J., and Duchet, J-C., J. Catal. 145, 429 (1994).

29. Afanasiev, P., Xia, G. F., Berhault, G., Jouguet, B., and Lacroix, M., Chem. Mater. 11, 3216 (1999).

30. Pollack, S. S., Sanders, J. V., and Tischer, R. E., Appl. Catal. 8, 383 (1983).

31. Alonso, G., Del Valle, M., Cruz, J., Petranovskii, V., Licea-Claverie, A., and Fuentes, S., Catal. Today 43, 117 (1998).

32. Rueda, N., Bacaud, R., and Vrinat, M., J. Catal. 169, 404 (1997).

33. Peureux, S., Bonnamy, S., Fixari,B., Lambert, F., Le Perchec, P., Pepin-Donat, B., and Vrinat, M., Bull. Soc. Chim. Belg. 104(4–5), 359 (1995).

34. Vissers, J. P. R., Groot, C. K., van Oers, E. M., de Beer, V. H. J., and Prins, R., Bull. Soc. Chim. Belg. 93, 813 (1984).

35. Vissers, J. P. R., Scheffer, B., de Beer, V. H. J., Moulijn, J. A., and Prins, R., J. Catal. 105, 277 (1987).

36. Jacobson, A. J., and Chianelli, R. R., U.S. Patent 4,650,563 (1987).

37. Lee, J. S., and Boudart, M., Appl. Catal. 19, 207 (1985).

38. Markel, E. J., and van Zee, J.W., J. Catal. 126, 643 (1990).

39. Ramanathan, S., and Oyama, S. T., J. Phys. Chem. 99, 16365 (1995).

40. Lee, K. S., Abe, H., Reimer, J. A., and Bell, A. T., J. Catal. 139, 34 (1993).

41. Schlatter, J. C., Oyama, S. T., Metcalfe, J. E., and Lambert, J. M., Ind. Eng. Chem. Res. 27, 1648 (1988).

42. Ranhotra, G. S., Bell, A. T., and Reimer, J. A., J. Catal. 108, 40 (1987).

43. Lee, J. S., Locatelli, S., Oyama, S. T., and Boudart, M., J. Catal. 125, 157 (1990).

44. Pham-Huu, C., Ledoux, M. J., and Guille, J., J. Catal. 143, 249 (1993).

45. Levy, R. L., and Boudart, M., Science 181, 547 (1973).

46. Chadwick, D., and Breysse, M., J. Catal. 71, 226 (1981).

47. Sivasanker, S., Ramaswamy, A. V., and Ratnasamy, P., “Proceedings of the 3rd International Conference on the Chemistry and Uses of Molybdenum” (M. F. Barry and P. C. H. Mitchell, Eds.), p. 98. Climax Molybdenum Co., 1979.

48. Tanaka, K. I., and Okuhara, T., Catal. Rev. Sci. Eng. 15, 249 (1977).

49. Salmeron, M., Somorjai, G. A.,Wold, A., Chianelli, R. R., and Liang, K. S., Chem. Phys. Lett. 90(2), 105 (1982).

50. Farias, M. H., Gelman, A. J., Somorjai, G. A., Chianelli, R. R., and Liang, K. S., Surf. Sci. 140, 181 (1984).

51. Kasztelan, S., C. R. Acad. Sci. Paris Ser. II 307, 727 (1988).

52. Faye, P., Payen, E., and Bougeard D., J. Catal. 179, 560 (1998).

53. Raybaud, P., Hafner, J., Kresse, G., and Toulhoat, H., Surf. Sci. 407, 237 (1998).

54. Wyckoff, R., “Crystal Structures,” 2nd ed., Vol. 1, p. 280, Interscience, New York, 1964.

55. Raybaud, P., Kresse,G., Hafner, J., and Toulhoat, H., J. Phys. Condens. Matter 9, 11085 (1997).

56. Topsøe, H., and Clausen, B. S., Catal. Rev. Sci. Eng. 26, 395 (1984).

57. Kelty, S. P., Li, J., Chen, J. G., Chianelli, R. R., Ren, J., and Whangbo, M. H., J. Phys. Chem. B 103, 4649 (1999).

58. Lee, J. S., Volpe, L., Ribeiro, F. H., and Boudart, M., J. Catal. 112, 44 (1988).

59. Raybaud, P., Hafner, J., Kresse,G., and Toulhoat, H., J. Phys. Condens. Matter 9, 11107 (1997).

60. Lacroix, M., Dumonteil, C., and Breysse, M., Prepr. Am. Chem. Soc., Div. Pet. Chem. 43(1), 35 (1998).

61. Berhault, G., Lacroix, M., Breysse, M., Maug´ e, F., Lavalley, J-C., and Qu, L., J. Catal. 170, 37 (1997).